

Comb and Branch-on-Branch Model Polystyrenes with Exceptionally High Strain Hardening Factor SHF > 1000 and Their Impact on Physical Foaming

Lorenz Faust, Marie-Christin Röpert, Masood K. Esfahani, Mahdi Abbasi, Valerian Hirschberg, and Manfred Wilhelm*


The influence of topology on the strain hardening in uniaxial elongation is investigated using monodisperse comb and dendrigraft model polystyrenes (PS) synthesized via living anionic polymerization. A backbone with a molecular weight of $M_{w,bb} = 310 \text{ kg mol}^{-1}$ is used for all materials, while a number of 100 short (SCB, $M_{w,scb} = 15 \text{ kg mol}^{-1}$) or long chain branches (LCB, $M_{w,lcb} = 40 \text{ kg mol}^{-1}$) are grafted onto the backbone. The synthesized LCB comb serves as precursor for the dendrigraft-type branch-on-branch (bob) structures to add a second generation of branches (SCB, $M_{w,scb} \approx 14 \text{ kg mol}^{-1}$) that is varied in number from 120 to 460. The SCB and LCB combs achieve remarkable strain hardening factors (SHF) of around 200 at strain rates greater than 0.1 s^{-1} . In contrast, the bob PS reach exceptionally high SHF of 1750 at very low strain rates of 0.005 s^{-1} using a tilted sample placement to extend the maximum Hencky strain from 4 to 6. To the best of the authors' knowledge, SHF this high have never been reported for polymer melts. Furthermore, the batch foaming with CO_2 is investigated and the volume expansions of the resulting polymer foams are correlated to the uniaxial elongational properties.

1. Introduction

Branching in polymers—and especially long chain branching (LCB)—is well-known for providing melt strength in elongational flow.^[1–3] Consequently, this topological feature is widely

L. Faust, M.-C. Röpert, M. K. Esfahani, V. Hirschberg, M. Wilhelm
 Institute of Chemical Technology and Polymer Chemistry (ITCP)
 Karlsruhe Institute of Technology (KIT)
 Engesserstraße 18, 76131 Karlsruhe, Germany
 E-mail: manfred.wilhelm@kit.edu

M. Abbasi
 Borealis Polyolefine GmbH
 Innovation Headquarters
 Linz 4021, Austria

 The ORCID identification number(s) for the author(s) of this article can be found under <https://doi.org/10.1002/macp.202200214>

© 2022 The Authors. Macromolecular Chemistry and Physics published by Wiley-VCH GmbH. This is an open access article under the terms of the Creative Commons Attribution-NonCommercial License, which permits use, distribution and reproduction in any medium, provided the original work is properly cited and is not used for commercial purposes.

DOI: 10.1002/macp.202200214

used in polymer processing like foaming, where elongational deformation occurs. For instance, during the bubble growth phase the presence of branching induces strain hardening, stabilizes the cell walls against local inhomogeneities in thickness and prevents premature cell wall rupture and coalescence, resulting in higher cell densities and volume expansions.^[4]

Strain hardening is identified in uniaxial extensional rheology as a rise of the extensional viscosity, η_E^+ , above the linear viscoelastic prediction.^[1,5] This non-linear melt property is quantified by the strain hardening factor (SHF), often referring to the ratio of the maximum achievable extensional viscosity to the linear viscoelastic (LVE) behavior ($\text{SHF} \equiv \eta_{E,\text{max}}^+ / \eta_{LVE,\text{max}}^+$).^[6–8] Alternative definitions use the non-linear response predicted by the Doi-Edwards (DE) model instead of the LVE envelope ($\text{SHF} \equiv \eta_{E,\text{max}}^+ / \eta_{DE,\text{max}}^+$).^[3,9] Typical values of the SHF for commercial branched polymers, e.g., low-density polyethylene (LDPE)

and LCB polypropylene (PP) are in the range of 10–20 and ≈ 50 , respectively.^[9–12] The extent of strain hardening is strongly correlated with the expandability of physically blown polymer foams for achieving cellular materials with low densities.^[13,14]

We are interested to study how melt rheological behavior modified by chain branching impacts foaming characteristics. The branching content is commonly varied by changing the chain topology, or other structural parameters as well as by blending. However, the majority of studies in literature use commercial polymers with an unknown topology or branching methods that produce rather polydisperse and structurally ill-defined systems that are poorly characterized. Thus, branching might be roughly quantified, but precise structural information like chain lengths and branching numbers and their specific impact on non-linear deformation in elongational experiments or processing remain unknown. In consequence, the optimization of the polymer on a molecular level with respect to specific macroscopic properties is rendered nearly impossible.

Several studies previously compared the foamability of linear and LCB isotactic polypropylene (*i*-PP) as well as blends thereof, and concluded that polymer melts with a higher branching content achieved a lower foam density, i.e., higher volume

expansion ratio (VER), a more homogenous cell morphology and smaller cell sizes. Simultaneously, the higher branched grades exhibit an increased strain hardening in elongational flow, indicating a higher melt strength that is also important for bubble stability.^[12,13,15]

Using *i*-PP for the investigation of structure–properties relationships reveals another disadvantage besides the unspecified branching structure. Semi-crystalline polymers, e.g., PE and *i*-PP, make it difficult to separate between effects caused by branching, crystal morphologies, or crystallization during non-isothermal processing conditions.

Just recently, Weingart et al.^[16] compared the foam qualities of linear and LCB extrusion processed *i*-PP. Even though only the LCB *i*-PP indicated superior melt strength by its elongational performance, the linear *i*-PP without any strain hardening achieved a lower foam density and smaller, more homogenous cell sizes. Those findings questioned “[...] The Legend of Strain-Hardening as a Requirement for Good Foamability”.^[16] However, the authors explained the unexpected result by a crystallization and gelation behavior that is more favorable for the linear *i*-PP when it comes to foam qualities in extrusion foaming. Nevertheless, the presented findings emphasize the necessity to investigate the effect of topology independently by using well-defined amorphous polymers.

López-Barrón et al.^[6,7] compared the extensional properties of a series of ultrahigh molecular weight poly(α -olefins) with densely grafted bottlebrush structures and different side group lengths to atactic polypropylene (*a*-PP). They found that a poly(1-octadecene) with the longest carbon number of 16 had the highest SHF of 80, over one order of magnitude higher than linear *a*-PP. Unfortunately, the relation between the elongational rheology and the foaming performance was not further investigated.

A similarly high SHF of 100 was also reached by Liu et al.^[17] who anionically synthesized centipede-like LCB PS with two branches per equally spaced branch point. However, despite only eight branch points giving a relatively low total number of branches ($N_{br} = 2 \times 8$), the high branch and backbone molecular weights ($M_{w,br} = 140 \text{ kg mol}^{-1}$ and $M_{w,bb} \approx 2700 \text{ kg mol}^{-1}$) resulted in a zero-shear viscosity, η_0 , of more than 10^9 Pa s (at $150 \text{ }^\circ\text{C}$), which is impractically high for melt processing applications.

In previous studies of our group, Abbasi and co-workers^[18–20] used anionic polymerization to synthesize a series of monodisperse atactic LCB comb PS with the same backbone length ($M_{w,bb} = 290 \text{ kg mol}^{-1}$) and similar, well-entangled branch length ($M_{w,br} = 44 \text{ kg mol}^{-1} \approx 3 M_e$), but varying number of branches per backbone, N_{br} , from 3 to 190. Those comb PS covered a wide range of conformational regimes from loosely grafted to densely grafted combs and loosely grafted bottlebrush conformations.^[21] Nonlinear, extensional properties in the form of the strain hardening factor (SHF) were correlated to the final foam characteristics with respect to the volume expansion ratio (VER) after batch foaming with supercritical CO_2 . Abbasi et al. found the optimum N_{br} was about 100, spaced 30 monomers apart on average, which resulted not only in a maximum SHF of about 200, but also a maximum expandability with a VER of about 40. This value is close to the theoretical limit considering the solubility of CO_2 in PS at the applied conditions. A further increase in N_{br}

to approach bottlebrush-like structures caused adverse effects in elongational and foaming performance with a concomitant decrease in SHF and VER. It was concluded that excessive branch crowding and tight space between the branch point segments along the backbone reduced the number of inter-chain entanglements with branches of neighboring comb molecules.^[22,23] Furthermore, the dynamic tube dilution was expected to decrease the effective number of entanglements along the backbone.^[18,19] Therefore, even though branching is known to have a positive impact on strain hardening, it was shown that, for the given model system above a certain number of side chains, the elongational performance in uniaxial extension as well as foam expansion is negatively affected. Consequently, excessive side chain crowding will not further increase the SHF.

Furthermore, also the side chain length seems to restrict the extensional performance, as just recently reported by Röpert et al.^[24] on the example of POM-POM-shaped PS with the same backbone length ($M_{w,bb} = 100 \text{ kg mol}^{-1}$) and approximately the same number of arms (≈ 11 – 14) per star, but varying arm length, $M_{w,a} = 9$ – 300 kg mol^{-1} . In this series, the highest SHF of 43 was achieved by a POM-POM having just well-entangled arms of $M_{w,a} = 50 \text{ kg mol}^{-1} \approx 3 M_e$, whereas elongation of samples with longer arms resulted in reduced strain hardening due to premature elastic rupture.^[24]

Dendrigraft polymers offer another way to increase the branching content, but are—up to now—not sufficiently explored when it comes to their melt properties,^[25–28] especially in elongational deformation.^[26–28] Those topologies, belonging to the dendritic polymer family, have a branch-on-branch (bob) structure. However, in contrast to highly defined dendrimers and ill-defined hyperbranched polymers, they possess semi-controlled polymeric branch units with a substantial ability to entangle.^[29–31]

Van Ruymbek et al.^[27] and Huang et al.^[28] investigated the uniaxial extension of symmetric model Cayley-tree PMMAs using a Sentmanat Extensional Rheometer (SER) and a Filament Stretch Rheometer (FSR) instrumentation, respectively. Those dendritic topologies with 4-arm star core and a regular branching with a multiplicity of two showed increased strain hardening with increasing number of graft generations (G). Whereas the transient extensional viscosity of a second-generation (G2) PMMA Cayley-tree only slightly increased above the LVE envelope, further generations (G3 and G4) achieved SHF in the range of 4–7 at low strain rates of about $\dot{\epsilon}_H = 10^{-1}$ – 10^{-3} s^{-1} . It is important to mention that the branch segments of each generation were low in molecular weight, $M_s = 11 \text{ kg mol}^{-1}$, with just two entanglements (using an entanglement molecular weight of $M_e = 4.55 \text{ kg mol}^{-1}$), giving a total M_w of only 380 kg mol^{-1} (G3) and 600 kg mol^{-1} (G4).^[27,28] Furthermore, the globular structure is less favorable in terms of chain extension and orientation—the origin of strain hardening.^[3,5,30] Unfortunately, elongational experimental data of other model branch-on-branch structures is scarce, a likely result of the high synthetic effort and lack of adequate sample quantities.

The synthetic strategy of backbone functionalization and successive side chain grafting offers a straightforward route not only to comb polymers, but also to dendrigraft polymer architectures, where each branching layer serves as a precursor for higher-generation branching. In a divergent manner the cycle

of functionalization, living anionic polymerization and grafting-onto can be repeated several times and high molecular weights of above 10^7 g mol⁻¹ can be attained within only few grafting cycles, as demonstrated for dendrigraft polystyrenes,^[32,33] polyisoprenes^[34] and polybutadienes,^[35] as well as various copolymer compositions.^[31,36]

The synthesis of homopolymer branch-on-branch polystyrenes (bob PS) from comb PS presented here is based on the Friedel–Crafts (FC) acetylation approach first described by Li and Gauthier^[33] who synthesized two series of “arborescent graft polystyrenes” with up to three grafting generations, each with side chains of 5 and 30 kg mol⁻¹, respectively. However, they started with rather short backbones of also 5 and 30 kg mol⁻¹.

In this work, a comb PS with well-entangled backbone of $M_{w,bb} = 310$ kg mol⁻¹ and densely grafted LCB of $M_{w,lc} = 40$ kg mol⁻¹ was synthesized as a precursor for the successive grafting with a second layer of barely entangled short chain branches (SCB) of $M_{w,sc} \approx 14$ kg mol⁻¹, leading to a series of bob PS with comb-like aspect ratio but different density of SCB corona. Furthermore, a SCB comb PS with also barely entangled side chains of $M_{w,sc} = 15$ kg mol⁻¹ served for comparison with the LCB comb. The SHF was quantified by uniaxial extensional rheology using the standard horizontal sample placement to the extensional viscosity fixture (EVF) device. Due to the high stretchability of bob PS, a modified sample placement to the EVF with a tilted angle of 20° was used to extend the range of accessible Hencky strains from $\epsilon_H = 4$ to 6 by adapting the idea of an oblique sample positioning as just recently published by Parisi et al.^[37] Finally, the samples were batch foamed with supercritical CO₂ at saturation pressures of 180 bar and within foaming temperatures of $T_{foam} = 125$ – 145 °C. The relationship between the branching structure and foam characteristics was investigated, using the SHF to identify influential factors affecting the foam properties, especially the relation to the resulting VER.

2. Experimental Section

2.1. Synthesis

Comb PS and dendrigraft-type branch-on-branch (bob) PS were synthesized using anionic polymerization and high vacuum techniques. A monodisperse linear PS with molecular weight $M_{w,bb} = 310$ kg mol⁻¹ was used as the backbone and Friedel–Crafts (FC) acetylated, resulting in a degree of functionalization of 6% corresponding to an average number of $N_{ac} = 167$ acetyl groups randomly distributed per backbone chain. In a next step, living PS side chains with a molecular weight of $M_{w,sc} = 15$ kg mol⁻¹ and $M_{w,lc} = 40$ kg mol⁻¹ were independently polymerized and each anion separately grafted in a nucleophilic addition reaction with the carbonyl groups onto the acetylated backbone. The resulting comb PS with a number of N_{sc} or $N_{lc} \approx 100$ short or long chain branches, are denoted as SCB comb PS310-100-15 ($PSM_{w,bb} - N_{sc} - M_{w,sc}$) and LCB comb PS310-100-40 ($PSM_{w,bb} - N_{lc} - M_{w,lc}$), respectively. Thus, on the basis of a similar set of molecular parameters in previous LCB comb PS, the number of entanglements of the backbone segments between two branch points, $Z_s \approx 0.2$, was presumed to be optimal for high SHF and VER.^[23] Details of the synthesis of comb PS and purifi-

cation by precipitation fractionation method have already been presented in previous publications.^[18,38] LCB comb PS310-100-40 was used as the precursor for the next branching generation and the cycle of functionalization and grafting-onto step was repeated to achieve bob PS, as schematically illustrated in **Figure 1**.

The comb PS was FC acetylated with about 0.5–2 mol% functionalization (Figure 1a). The SCB with a $M_{w,sc} \approx 14$ kg mol⁻¹ were synthesized separately using anionic polymerization methods (Figure 1b). The final grafting-onto step with the living SCB onto the functionalized LCB resulted in the dendrigraft-type bob PS (Figure 1c), of which bob PS310-100-40-g-120-14 with the lowest grafting density of 120 SCB is shown as a representative example for average numbers and length scales. In total, a series of three bob PS samples (denoted $PSM_{w,bb} - N_{lc} - M_{w,lc} - g - N_{sc} - M_{w,sc}$) with different outer SCB density were synthesized, having a total number of $N_{sc} = 120$, 240, and 460 SCB while keeping the length of those branches with about 14 kg mol⁻¹ constant. The achieved grafting yields of 57–66% were consistent with reports of Li and Gauthier,^[33] who found a conversion of only 2/3 of acetyl functional groups into branch points due to enolate formation as competing side reaction.

As previously described, the acetylation is a random process, so new acetyl groups are also created on the backbone of comb PS310-100-40. However, due to the low volume fraction of the backbone of $\phi_{bb} \ll 10$ mol% in the comb, statistically > 90% of the functional groups will be found on the LCB of comb PS310-100-40, and therefore also > 90% of the additional SCB of the second grafting stage will be attached onto the comb PS side chains. Considering the easier steric accessibility of the peripheral side chains versus backbone, grafting is expected to take place more favorably onto the existing branches of the comb. Due to the random, regio-unselective acetylation, the position of the SCB on the LCB underlies also a variation. Apart from being—ideally—grafted mid-chain of the LCB, the SCB can also be attached to the apex of the LCB resulting in a (nearly) linear, extended LCB of ≈ 55 kg mol⁻¹, or grafted close to the backbone, resembling a centipede- or barbwire-like branch point.

2.2. Molecular Characterization

Proton NMR spectra were used to analyze the degree of functionalization after the FC acetylation reaction. The molecular weights of the backbone, side chains, and combs were determined using size exclusion chromatography (SEC). Additionally, the molecular weights of the comb and bob PS were determined gravimetrically, using molecular information from SEC and NMR.

2.2.1. ¹H-NMR

The ¹H-NMR spectra were measured in deuterated chloroform at 25 °C using a 400 MHz Bruker Avance III Microbay spectrometer. The analysis of the NMR spectra and the calculation method to determine the degree of functionalization are described in detail by Abbasi et al.^[18] The calculated number of acetyl groups, N_{ac} , per backbone or comb precursor is given in Table S1 (Supporting Information).

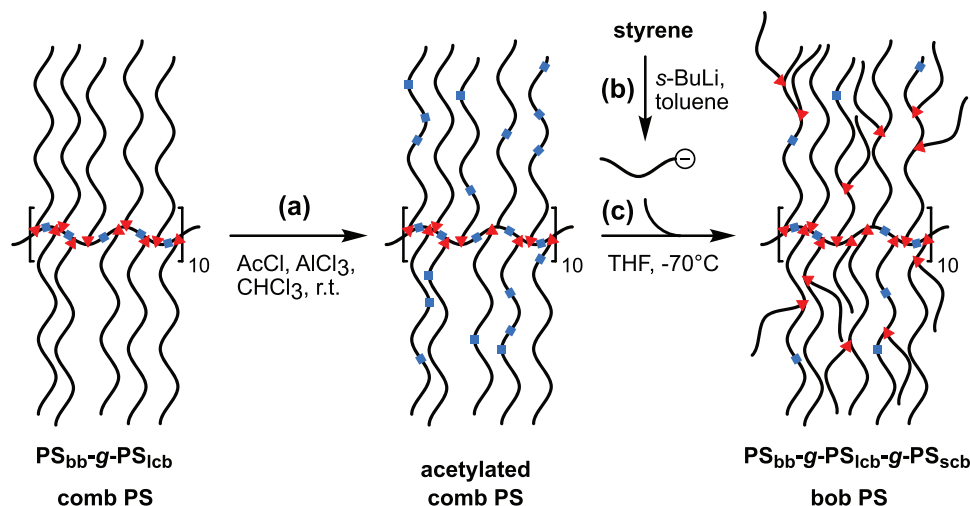


Figure 1. Reaction scheme for the synthesis of model branch-on-branch (bob) PS from comb PS. a) Friedel–Crafts (FC) acetylation of LCB comb PS310-100-40 to introduce carbonyl functional groups (blue ■). The comb PS precursor already has residual functional groups from previous grafting cycle, see Abbasi et al.^[18] b) Anionic polymerization of living SCB with $M_{w,scb} \approx 14 \text{ kg mol}^{-1}$. c) Grafting of SCB onto acetylated LCB. The carbonyl groups turn into branch points (red ▲). The illustrated synthesis of bob PS310-100-40-g-120-14 shows a representative example for average numbers and length scales. The nomenclature is explained in the text.

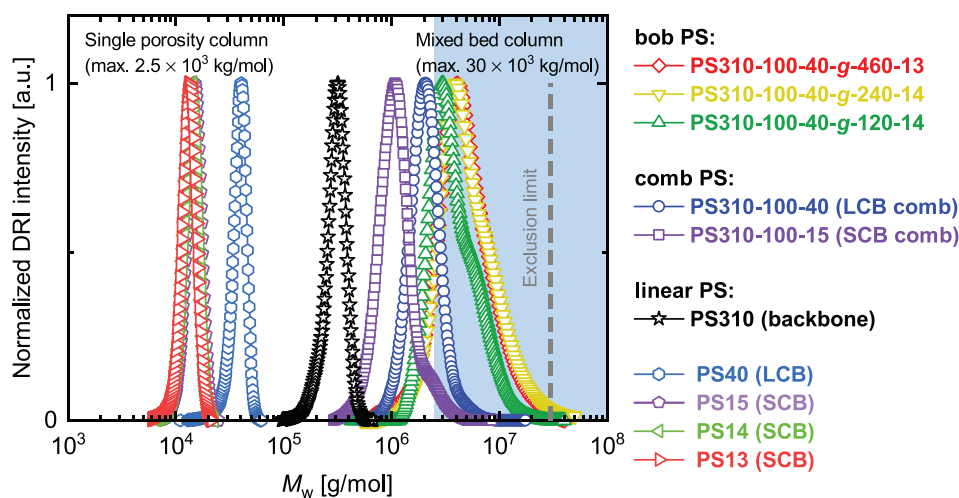


Figure 2. Molecular weight distribution profiles (normalized differential refractive index intensity vs molecular weight) of purified comb and bob PS polymers, using linear PS standard calibration. An analytical single porosity column (max. $2.5 \times 10^3 \text{ kg mol}^{-1}$) was used for the linear PS310 and the precursor graft SCB (PS15, PS14, PS13) and LCB (PS40) chains. A semi-preparative mixed bed column (max. $30 \times 10^3 \text{ kg mol}^{-1}$) was used for the comb and bob samples. The nomenclature is explained in the text.

2.2.2. SEC

The SEC equipment was from the Agilent 1200 series. The SEC measurements used THF as the mobile phase at $25 \text{ }^\circ\text{C}$ and a flow rate of 1 mL min^{-1} . The molecular weights of the linear PS310 backbone, SCB and LCB branches were determined with an analytical, single porosity column (PSS, SDV Lux 10^3 and $10^5 \text{ } \text{Å}$, $5 \text{ } \mu\text{m}$). Due to the exclusion limit of $2.5 \times 10^3 \text{ kg mol}^{-1}$, a preparative, mixed bed column (PSS, SDV XL $10^7 \text{ } \text{Å}$, $10 \text{ } \mu\text{m}$) with an exclusion limit of $30 \times 10^3 \text{ kg mol}^{-1}$ was used for the analysis of the comb and bob PS. The SEC columns were calibrated using linear PS standards as received from PSS GmbH (Mainz, Germany)

ranging from 476 to $14 \times 10^6 \text{ g mol}^{-1}$. **Figure 2** shows the molecular weight distribution profiles of the synthesized backbone, comb and bob PS as well as the separated SCB and LCB samples prepared before grafting reaction. Molecular weight characteristics of each structural component are presented in detail in **Table 1**.

2.2.3. Gravimetry

The mass difference between the purified comb or bob PS product recovered after precipitation fractionation, m_{gr} , and its respective acetylated linear or comb precursor before the grafting

Table 1. Molecular parameters of model comb and bob PS310 series. All molecular weights in kg mol⁻¹.

Sample name ^{a)}	Long chain branches			Short chain branches			Total			
	$N_{\text{lcb}}^{\text{b)}$	$M_{\text{wlcb}}^{\text{c)}$	$\bar{D}_{\text{lcb}}^{\text{c)}$	$N_{\text{sbc}}^{\text{b)}$	$M_{\text{wsbc}}^{\text{c)}$	$\bar{D}_{\text{sbc}}^{\text{c)}$	$M_{\text{w}}^{\text{d)}$	$M_{\text{n,SEC}}^{\text{c)}$	$M_{\text{w,SEC}}^{\text{c)}$	$\bar{D}_{\text{SEC}}^{\text{c)}$
PS310								290	310	1.14
PS310-100-15				103	15	1.03	1800	860	1150	1.33
PS310-100-40	98	39	1.03				4200	1630	2150	1.13
PS310-100-40-g-120-14	98	39	1.03	123	14	1.03	5900	3270	4240	1.30
PS310-100-40-g-240-14	98	39	1.03	236	14	1.03	7600	3850	6720	1.74
PS310-100-40-g-460-13	98	39	1.03	461	13	1.03	10 100	4310	5500	1.28

^{a)} Branch-on-branch (bob) PS samples labeled according to: $PSM_{\text{w,bb}}-N_{\text{lcb}}-M_{\text{wlcb}}-g-N_{\text{sbc}}-M_{\text{wsbc}}$; ^{b)} Number of branches calculated from gravimetric method; ^{c)} Apparent molecular weights in kg mol⁻¹ and dispersities determined by SEC using linear PS standard calibration; ^{d)} Total molecular weights calculated based on gravimetric results, $M_{\text{w}} = M_{\text{w,bb}} + N_{\text{lcb}} \times M_{\text{wlcb}} + N_{\text{sbc}} \times M_{\text{wsbc}}$.

reaction, m_{ac} , is directly attributed to the amount of grafted branches. Since the molecular weights of the acetylated precursor, $M_{\text{w,ac}}$, and grafted branches, $M_{\text{w,br}}$, are known, the average number of grafted branches, N_{br} , can be calculated according to Equation (1).

$$N_{\text{br}} = \frac{(m_{\text{gr}} - m_{\text{ac}}) M_{\text{w,ac}}}{m_{\text{ac}} M_{\text{w,br}}}$$

The gravimetrically determined values of m_{ac} and m_{gr} are summarized in Table S1 (Supporting Information) along with the results of the calculations of N_{br} , as well as the grafting yield, i.e., the fraction of carbonyl functional groups converted into branch points, $\text{mol}\%_{\text{gr}} = N_{\text{br}}/N_{\text{ac}}$. Furthermore, N_{br} is reported as the respective N_{lcb} or N_{sbc} in Table 1.

As a simple and straightforward method, the gravimetric analysis was previously used by Li and Gauthier^[33] to determine the grafting yield of second-generation “arborescent” (i.e., dendrigraft) PS that did not elute from the SEC column. When comparing the gravimetric method with the SEC trace method, they reported very good agreement with only about 2 percentage points deviation in grafting yields.

The accuracy of the gravimetric method is only ensured with high recovery purification. Due to the perfect baseline separation in the SEC (see Figure 2) and the 100- to 1000-fold factor difference in molecular weight between comb or bob PS versus precursor branches, an excellent fractionability with little to no loss of comb or bob PS mass could be achieved, as confirmed via SEC from the precipitate and supernatant phase. Within only 2–4 precipitation fractionation cycles, a high purity (>99%) and nearly full recovery of the branched product fraction was obtained.

The difference in molecular weights reported by the gravimetric method and the SEC characterization are attributed to both techniques giving absolute versus relative values, respectively. While the latter is based on the calibration of the column with linear PS standards, giving same molecular weights for same hydrodynamic radii, the former calculates the molecular weights directly obtained from the mass difference of the acetylated precursor before grafting and the purified product after fractionation.

Since branching increases the molecular density, the expected hydrodynamic radii are lower than compared to the gaussian

chain conformation of a linear chain with the same molecular weight. Therefore, it is evident that the apparent $M_{\text{n,SEC}}$ and $M_{\text{w,SEC}}$ values of comb PS are largely underestimated. This underestimation is even more the case for dendrigraft PS with additional, outer SCB on top of the inner LCB. For example, the SEC only reports a moderate increase in $M_{\text{n,SEC}}$ from 3300 to 4300 kg mol⁻¹ when comparing the bob PS with the lowest number of SCB ($N_{\text{sbc}} = 120$) with the highest number of SCB ($N_{\text{sbc}} = 460$), even though the number of outer SCB nearly quadruples.

2.3. Rheological Characterization

Linear viscoelastic (LVE) properties were measured via small amplitude oscillatory shear (SAOS) deformation using an ARES-G2 rheometer (TA Instruments) and parallel plate geometry with a diameter of $d = 13$ mm and a gap of $h \approx 1$ mm. The measurements were performed within an angular frequency range from $\omega = 100$ to 0.01 rad s⁻¹ and a temperature range between 130 and 240 °C. The LVE mastercurves were obtained by applying the time-temperature superposition (TTS) principle and shifted to a reference temperature of $T_{\text{ref}} = 180$ °C using the WLF equation $\log a_T = -C_1(T - T_{\text{ref}})/(C_2 + T - T_{\text{ref}})$.

In order to assess the thermorheological stability of the PS samples, time sweep tests at $\omega = 80$ rad s⁻¹ and a strain amplitude of $\gamma_0 = 4.5\%$ were performed on the example of comb PS310-100-40 at 200 °C over a duration of 15 h. Repeated frequency sweep tests showed reproducible results compared to the former SAOS mastercurve with a reduction in storage and loss moduli, G' and G'' , of less than 5%. The structural stability of branched PS was confirmed by SEC measurements before and after rheological tests, with changes of less than 5% in M_{w} or \bar{D} .^[39]

The LVE data in the frameworks of the absolute value of the complex viscosity, $|\eta^*|$, along with Maxwell model fittings is shown in Figure S1 (Supporting Information). The zero-shear viscosities, η_0 , were calculated by extrapolating the relaxation spectra data (g_i and τ_i) to the low angular frequency region, $\eta_0 = \sum g_i \tau_i$, and reported in Figure S2 (Supporting Information).

Uniaxial extensional measurements were performed on an extensional viscosity fixture (EVF) geometry at a temperature of 180 °C and at different extensional rates between $\dot{\epsilon}_{\text{H}} = 10^{-3}$ and

10 s^{-1} . The standard EVF setup on the ARES-G2 with horizontal sample placement allows a maximum deformation of Hencky strain of $\epsilon_{\text{H}} = 4$.^[40] Additionally, to extend the recordable deformation range of highly stretchable samples to a maximum of $\epsilon_{\text{H}} = 6$, extensional measurements were performed using a modified sample placement with a tilted angle of 20° on the drums of the EVF with respect to the horizon.^[37] Due to the start of the rotation in a tilted position and the sample angle approaching zero as the time increases, based on the geometric relations of the force components acting perpendicular on the drums, the material stress was corrected from the recorded instrument stress data with respect to the sample angle change over time.

Extensional experiments were repeated in case of a discrepancy between the extensional viscosity at the early stage of stretching (i.e., start-up extensional viscosity) and the LVE prediction from the Maxwell model fitting, $\eta_{\text{E}}^+ = 3 \sum g_i \tau_i (1 - \exp(-t/\tau_i))$, using relaxation spectra.

2.4. Foaming Experiments and Analysis

Foaming experiments were performed in an autoclave system as pressure induced (one-step) batch foaming process with CO_2 as the physical foaming agent. The purified and dried PS samples were press-molded under vacuum at 180°C into disks with 10 mm diameter and 2 mm thickness. The samples were placed in the autoclave system (modified benchtop mini reactor, Type 4560, Parr Instruments) and saturated with CO_2 at supercritical conditions of 180 bar. The saturation and foaming conditions were varied within a temperature range of $T_{\text{foam}} = 125\text{--}145^\circ\text{C}$. In previous studies, those foaming conditions already proved as optimum foaming window for the autoclave system to maximize the volume expansion (with a theoretical limit of $\text{VER} \approx 45 \pm 5$ due to the maximum CO_2 solubility) and correlate the uniaxial extensional rheology to the foaming properties.^[22,23] After a saturation time of 4 h, the foaming was induced by sudden depressurization at an average rate of about 40 bar s^{-1} .

Densities of the neat polymer and foam, ρ_{neat} and ρ_{foam} , respectively, were measured via the principle of buoyancy using a density kit (YDK 01-0D, Sartorius) on the balance and the volume expansion ratio, $\text{VER} = \rho_{\text{neat}}/\rho_{\text{foam}}$, was calculated accordingly. Scanning electron microscopy (SEM, S5-70, Hitachi) was used to reveal the cellular structure. The cell densities and average cell sizes were analyzed via the software ImageJ using images with about 200–500 cells. The calculation of the cell density, N_{cell} , in cell cm^{-3} and average cell diameter, d_{cell} , in μm is described in previous publications.^[22,23]

3. Results and Discussion

3.1. Uniaxial Extensional Rheology

3.1.1. Standard Horizontal Sample Placement for Hencky Strains up to 4

To analyze the influence of topology on the strain hardening behavior of the linear and branched polymer melts, we first measured uniaxial extensional rheology with the standard horizontal sample placement on the EVF geometry.

Figure 3 shows the extensional viscosity, η_{E}^+ , versus stretch time, t , for different extensional rates. While the linear PS310 (Figure 3a) showed barely any strain hardening with only a slight upward deviation of the extensional viscosity from the LVE envelope at very high elongational strain rates ($\dot{\epsilon}_{\text{H}} = 10 \text{ s}^{-1}$), the presence of even slightly entangled SCB of about one entanglement molecular weight, $M_{\text{w,scb}} \approx 1 M_{\text{e}}$, in comb PS310-100-15 (Figure 3b) induced significant strain hardening on the order of two decades. An increase in the length of side chains toward comb PS310-100-40 (Figure 3c) with well-entangled LCB of $M_{\text{w,lc}} \approx 2.8 M_{\text{e}}$ not only reduced the onset extensional rate of strain hardening about one decade (from $\dot{\epsilon}_{\text{H}} = 0.1$ to 0.01 s^{-1}), but also shifted the range of strain rates with maximum strain hardening about two decades lower. Grafting of additional SCB onto LCB comb PS310-100-40 (Figure 3d–f) further reduced the onset of strain hardening toward extensional rates as low 0.001 s^{-1} . More significantly, the presence of dendritic branching drastically increased the strain hardening properties with the extensional viscosity exceeding the LVE envelope by over two decades. However, especially at low deformational rates ($\dot{\epsilon}_{\text{H}} < 0.03 \text{ s}^{-1}$) dendrigraft-type bob PS exhibit very high stretchability with an almost unobtainable steady-state extensional viscosity before a Hencky strain of $\epsilon_{\text{H}} = 4$, which is the limit for reliable transient viscosity data due to the instrumental design of the EVF geometry. After one revolution of the geometry cylinders, the stretching filament touches the sample ends and starts to wind up on itself, leading to a non-uniform deformation due to a sudden increase of the effective cylinder diameter.^[40] The pronounced stretchability was especially observed for bob PS310-100-40-g-120-14, whose extensional viscosity data, η_{E}^+ , for the lowest strain rate of $\dot{\epsilon}_{\text{H}} = 0.001 \text{ s}^{-1}$ is exemplarily displayed over the full elongation time in Figure 3d. The maximum steady-state extensional viscosity would only be reached beyond $\epsilon_{\text{H}} > 4$ (grayed out data points), rendering an accurate quantification of the strain hardening impossible. Therefore, the ultimate strain hardening of the sample when calculated only up to $\epsilon_{\text{H}} = 4$ is assumed to be grossly underestimated. To overcome the experimental difficulties in measuring highly stretchable samples, the procedure of an oblique sample positioning, presented by Parisi et al.^[37] as an alternative use of the Sentmanat Extensional Rheometer (SER), was adapted to the EVF geometry, as further addressed in Section 3.1.2.

Although the steady-state elongational viscosity and the simulation of the raw data with constitutive models is of high academic interest in fundamentally understanding chain dynamics in elongational deformation,^[3,11,41] the degree of strain hardening as the quantification of melt stability is of high practical relevance from a processing perspective.^[6,7]

Figure 4 summarizes the extensional viscosity data in the framework of the strain hardening factor as the ratio of the maximum achievable extensional viscosity to the nonlinear response predicted by the Doi-Edwards (DE) model, $\text{SHF} \equiv \eta_{\text{E,max}}^+/\eta_{\text{DE,max}}^+$.^[3,18]

The analysis of the experimentally observed strain hardening reveals that comb PS310-100-15 with barely entangled side chains excels with very high $\text{SHF} > 100$ in the range of high elongational strain rates ($\dot{\epsilon}_{\text{H}} \geq 1 \text{ s}^{-1}$). At $\dot{\epsilon}_{\text{H}} = 10 \text{ s}^{-1}$ the SCB comb reaches a $\text{SHF} > 200$ for Hencky strains below 4. This tremendous effect of branching on the SHF of comb PS has so far only been reported by Abbasi et al.^[18,20,23] for a LCB comb PS290-120-44 with

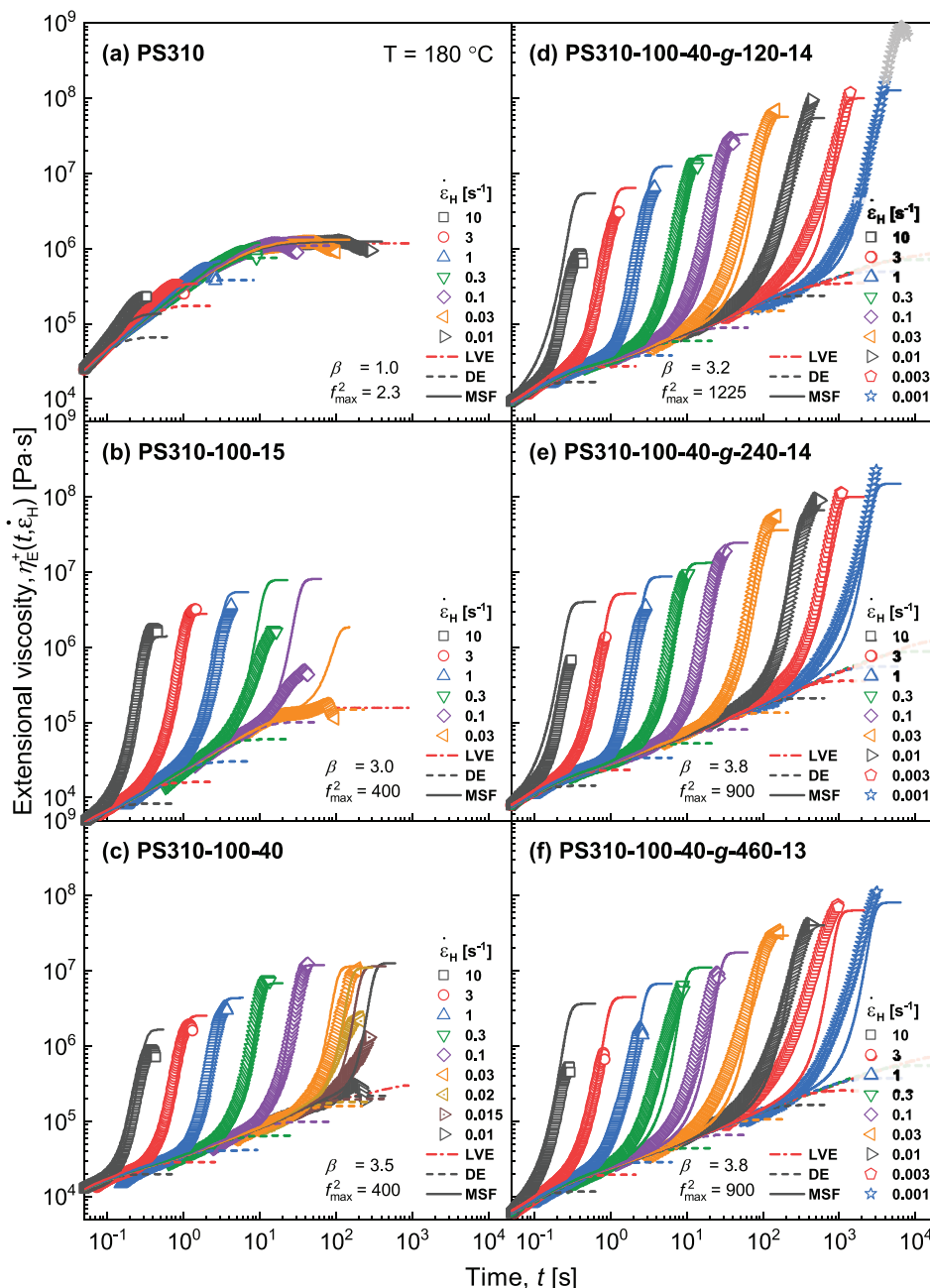


Figure 3. Uniaxial extensional viscosity, η_E^+ , at different extensional rates and $T = 180\text{ }^\circ\text{C}$, along with predictions from the DE model (dashed lines) and MSF model (solid lines). a) Linear PS310. b) SCB comb PS310-100-15. c) LCB comb PS310-100-40. d,e) Bob PS with 120, 240, and 460 additional SCB on LCB. All data is reported up to a Hencky strain of $\epsilon_H = \dot{\epsilon}_H \cdot t = 4$, the experimental limit of the EVF geometry. Greyed out data in (d) at $\dot{\epsilon}_H = 0.001\text{ s}^{-1}$ exceeds $\epsilon_H > 4$, but exemplarily shows the high stretchability of bob PS310-100-40-g-120-14.

well-entangled side chains of 44 kg mol^{-1} and similar backbone length and branching number, however, at much lower strain rates of 0.1 s^{-1} . In comparison with the newly synthesized comb PS310-100-40 possessing similar structural features, the results are consistent as both LCB combs show their maximum SHF at the same rate of 0.1 s^{-1} . Moreover, with 100 LCB achieving a slightly lower SHF = 130, the extensional properties of PS310-100-40 are between that of combs PS290-60-44 (SHF ≈ 100) and PS290-120-44 (SHF ≈ 200).^[18] Additionally, the LCB of PS310-

100-40 are about 10% shorter which might also contribute to a somewhat decreased SHF.

The grafting of SCB chains onto the LCB comb structure, i.e., the conversion toward bob PS topology furthermore drastically changes the extensional properties, especially toward higher SHF at even lower strain rates. Whereas the SHF at high rates of 10 s^{-1} is barely affected by the additional presence of SCB, with both LCB comb and SCB bob PS having roughly the same SHF ≈ 50 , all bob PS samples exceed the comb's strain hardening

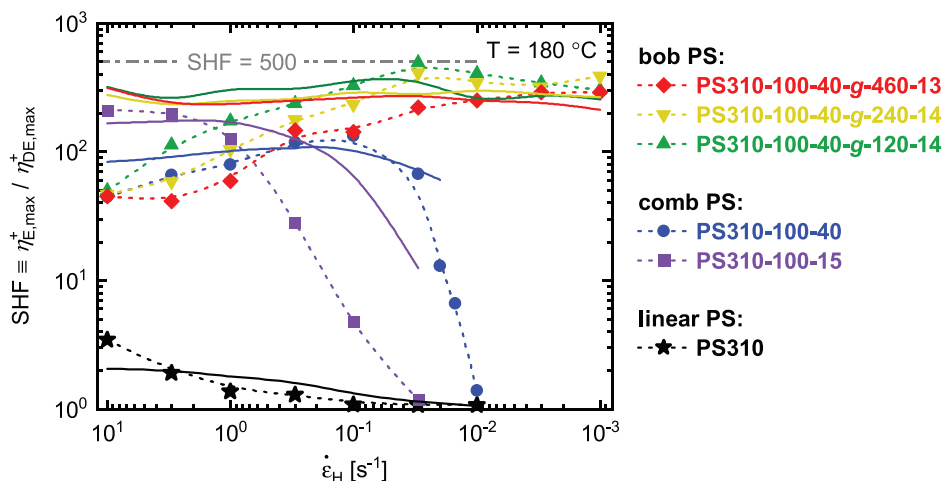


Figure 4. Strain hardening factor, $\text{SHF} \equiv \eta_{E,\text{max}}^+ / \eta_{DE}^+$, as a function of extensional rate, $\dot{\epsilon}_H$, from high to low strain rates. Symbols represent the maximum experimentally achieved extensional viscosity, $\eta_{E,\text{max}}^+$, up to a Hencky strain of $\epsilon_H = 4$. Dashed lines show the general trend as guide to the eye and solid lines are predictions of the MSF model.

properties at lower rates ($\dot{\epsilon}_H < 1 \text{ s}^{-1}$). Bob PS310-100-40-g-120-14 with the lowest SCB graft density achieves an exceptionally high maximum SHF of 500 at $\dot{\epsilon}_H = 0.03 \text{ s}^{-1}$ and a Hencky strain below 4. This is to the best of our knowledge a value that has not been reported before for a thermoplastic polymer melt. Interestingly, there seems to be a clear tendency toward somewhat lower strain hardening with more outer SCB. In contrast to the bob PS with $N_{br} = 120$, an increase to 240 or even 460 SCB resulted in decreasing SHF, with the latter two samples breaking mostly at Hencky strains below 4. Accordingly, both were more brittle in the melt state, but also challenging to handle during sample preparation due to their mechanical fragility in solid state. In this respect, the results are also consistent with findings by Abbasi et al.^[18,23] who showed at the example of comb PS290- N_{br} -44 series, that the highest density of LCB, e.g., $N_{br} = 190$ with bottlebrush-like side chain crowding, did not achieve the highest SHF. Consequently, this particular comb PS also performed worse in foaming when it comes to achieving low dense foams.^[23] It is assumed that above an optimum number of branches, a too high branch density impedes inter-chain interaction and results in inefficient entangling.^[18,23]

Nevertheless, all bob PS still achieved remarkable $\text{SHF} \approx 250\text{--}400$ at $\dot{\epsilon}_H \leq 0.01 \text{ s}^{-1}$. As already discussed above, the SHF values of bob PS310-100-40-g-120-14 at $\dot{\epsilon}_H \leq 0.01 \text{ s}^{-1}$ are most likely underestimated due to the stretchability of the samples surpassing the limitations of the EVF geometry regarding the maximum Hencky strain of 4. Unfortunately, comparison with experimental data of other model branch-on-branch structures is not possible due not only to a general lack of published samples but also to the dissimilarity in topology and parameters of branch number and size.

3.1.2. Tilted Sample Placement for Hencky Strains up to 6

The standard horizontal placement of the sample in the EVF fixture limits the deformation that can be performed to Hencky strains less than 4. After one full drum rotation, the sample ends meet the stretching filament and the effective drum diameter

suddenly increases. The strain becomes non-uniform and the recorded torque data no longer represents the uniaxial properties of the material.^[40]

As shown by Parisi et al.,^[37] placing a sample with an angle on the drums of a SER tool delays sample overlapping and circumvents the instrumental limitation in the deformation of highly stretchable elastomers or polymer melts. Applying the same principle on an EVF, the range of deformation can be extended to Hencky strains up to $\epsilon_H = 6$. The true time dependent material stress can be obtained after correcting the recorded instrument stress data by taking into account the angle change over time, and the extensional viscosity is calculated accordingly.

Figure 5 shows the extensional viscosity data for bob PS310-100-40-g-120-14 sample placed horizontally (blue squares) as well as in a 20° tilted angle with respect to horizon (red circles). An extensional rate of 0.005 s^{-1} deemed reasonably low to achieve a high stretchability of the sample at those condition to prove the feasibility of this method, however fast enough to mitigate sagging effects and sensitivity issues at 180°C . Whereas η_E^+ of the standardly placed sample exceeded the DE model prediction by three decades, i.e., $\text{SHF} = 600$ until $\epsilon_H = 3.9$, the filament in the modified approach only failed at $\epsilon_H = 5.5$, resulting in a nearly 3 times higher SHF of 1750. The perfect overlapping of both extensional viscosity curves signifies the validity and good reproducibility of the viscosity data obtained with those different approaches.

3.2. One-Step Batch Foaming

Linear, comb and bob PS samples were foamed to investigate the impact of extraordinarily high strain hardening on practical aspects like foaming characteristics that is influenced by extensional flow properties. Foaming experiments were conducted in a batch foaming autoclave at a saturation pressure of 180 bar and foaming temperatures, T_{foam} , between 125 and 145°C .

Figure 6 shows the SEM images of the cellular foam structures produced at increasing foaming temperature from 125°C (Figure 6a–d), to 135°C (Figure 6e–h), and 145°C (Figure 6i–l).

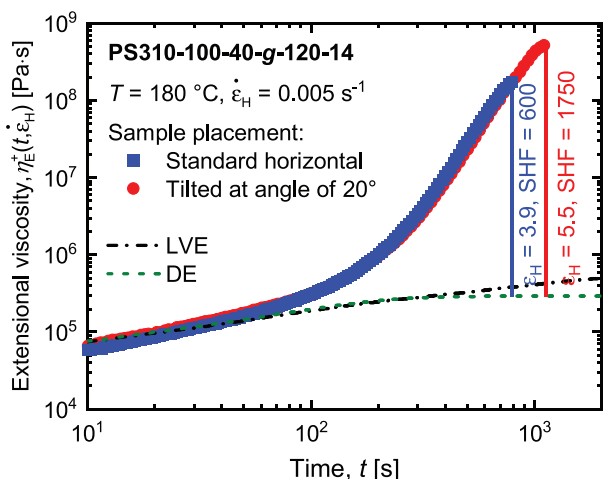


Figure 5. Comparison of uniaxial extensional viscosity data, η_E^+ , and SHF of bob PS310-100-40-g-120-14 at a Hencky strain rate of 0.005 s^{-1} at 180 °C for two different sample placement approaches using an EVF geometry on an ARES-G2 rheometer, along with the LVE envelope and DE model prediction. The standard horizontally placed sample reached a maximum SHF of 600 at $\epsilon_H = 3.9$ until the stretched filament started winding up on itself (blue squares). Attaching the sample by a tilted angle of 20° to the drums with respect to horizon delays this instrumental limitation and extended the recordable Hencky strain to $\epsilon_H = 5.5$ when the sample failed at a maximum SHF of 1750 (red circles).

In general, the foaming produced closed cell morphologies with cell diameters in the range of about $20\text{--}60 \mu\text{m}$. Linear PS310 was not able to expand to a stabilized foam at 145 °C and no cell structure could be analyzed at this condition (see Figure 6i), while at lower temperatures foaming could still be achieved. In contrast, all foams based on branched polymers showed foamability over the whole temperature range with relatively homogenous cell structure.

The results of the foam analysis are summarized in **Figure 7** as a function of the foaming temperature, with the average cell size, d_{cell} , and cell density, N_{cell} , as the microscopic properties (Figure 7a,b), as well as the foam density, ρ_{foam} , and volume expansion ratio, VER, as the macroscopic properties (Figure 7c,d).

Microscopically, the average cell diameters about doubled in size from $d_{\text{cell}} \approx 20\text{--}30$ to $40\text{--}60 \mu\text{m}$ with increasing temperature from 125 to 145 °C , with comb PS producing slightly larger cells compared to bob PS (Figure 7a). Conversely, cell densities that were on the order of $N_{\text{cell}} \approx 10^9 \text{ cell cm}^{-3}$ at the lowest temperature of 125 °C decreased with higher temperatures (Figure 7b), as also reported for the foaming of similar combs.^[23] This reduction of cell densities was most significant for the linear PS that dropped about one order of magnitude at 135 °C . At the highest temperature of 145 °C , the bob PS still achieved about two times higher cell densities than the combs.

When it comes to the macroscopic properties related to the foamability, at the lowest foaming temperature of 125 °C , all samples had roughly the same density of $\rho_{\text{foam}} \approx 0.1 \text{ g cm}^{-3}$. Minimum foam densities of about $0.03\text{--}0.04 \text{ g cm}^{-3}$ were achieved at higher foaming temperatures of $135\text{--}145 \text{ °C}$ for comb PS structures (Figure 7c). In a previous publication from our group, linear PS290 and LCB comb PS290- N_{br} -44 series had also nearly the same $\text{VER} \approx 10$ at 125 °C , independent of the presence of

branching or branching number from $N_{\text{br}} = 3$ to 190 .^[23] Of this series, foaming data of PS290-120-44 with similar structural features to PS310-100-40 is additionally shown. In comparison to the branched PS species, the expansion of PS310 is significantly lower, which failed to form a stable foam at 145 °C (Figure 7d). Only the branched PS that also exhibit strain hardening in uniaxial elongation were able to improve in VER at those conditions. Interestingly, the SCB and LCB combs, PS310-100-15 and PS310-100-40, respectively, most efficiently used the dissolved CO_2 gas for bubble growth and outperformed all the bob PS. Both combs achieved a maximum $\text{VER} \approx 40$, that was also found for comb PS290-120-44. This value is about 90% of the theoretical limit considering the solubility of CO_2 of $9 \pm 1 \text{ g CO}_2/100 \text{ g PS}$ at those conditions.^[23] The influence of topology on the foamability is more pronounced at the maximum foaming temperature of 145 °C , with bob PS only reaching half the values ($\text{VER} \approx 15\text{--}20$) of comb PS. Furthermore, it is remarkable that comb PS310-100-15 with only slightly entangled side chains and lowest zero-shear viscosity, $\eta_0 = 5 \times 10^{-4} \text{ Pa s}$ (Figure S2, Supporting Information), excelled in volume expansion at the highest temperature, whereas linear PS310 with an about a decade higher zero-shear viscosity was not even remotely able to result in a stabilized foam.

3.3. Correlation of the VER with Rheological Properties and Identifying Influential Factors

During the bubble growth phase of the foaming of a polymer melt, polymer chains at the bubble boundary undergo a biaxial deformation. In the early stage of the bubble growth, the cell walls, i.e., the distance between two boundary layers of neighboring bubbles, are comparably thick in contrast to the dimension of the bubble nuclei.^[42] At this stage, the expansion of the bubbles results in small local deformations of the polymer chains. Especially at increased distance from the boundary regions, the material behavior at those small deformations in biaxial extension is majorly governed by the linear viscoelastic regime.^[43,44] However, as the bubble growth progresses and the cell walls get thinner, the deformation increases and the biaxial deformation field mainly becomes nonlinear, controlled by the extensional viscosity. Strain hardening behavior is important for melt stability in elongational processes and consequently stabilizes the cell walls and enhances expandability to enable high VER.^[23] Strain hardening occurring in biaxial direction is also reflected in uniaxial extensional experiments that achieve high reproducibility of the data with relatively simple instrumentation.^[3,45] However, it should be mentioned that the intensity of strain hardening is higher in the uniaxial than the biaxial direction.^[8,46]

In the work presented here, comb-like structures with short and long chain branching, i.e., PS310-100-15 and PS310-100-40, respectively, that nearly achieved a maximum theoretical $\text{VER} \approx 30\text{--}40$, overall performed better in expandability than dendrigraft bob topologies, even though their maximum achievable SHF of $130\text{--}200$ was in general lower than bob PS with SHF of $300\text{--}600$ (measured up to $\epsilon_H = 3.9$) or even SHF of 1750 (measured with a modified EVF up to $\epsilon_H = 5.5$). In that sense, the higher SHF did not lead to a higher VER as expected from previous findings by Abbasi et al.^[23] At this point it is evident that for such a complex

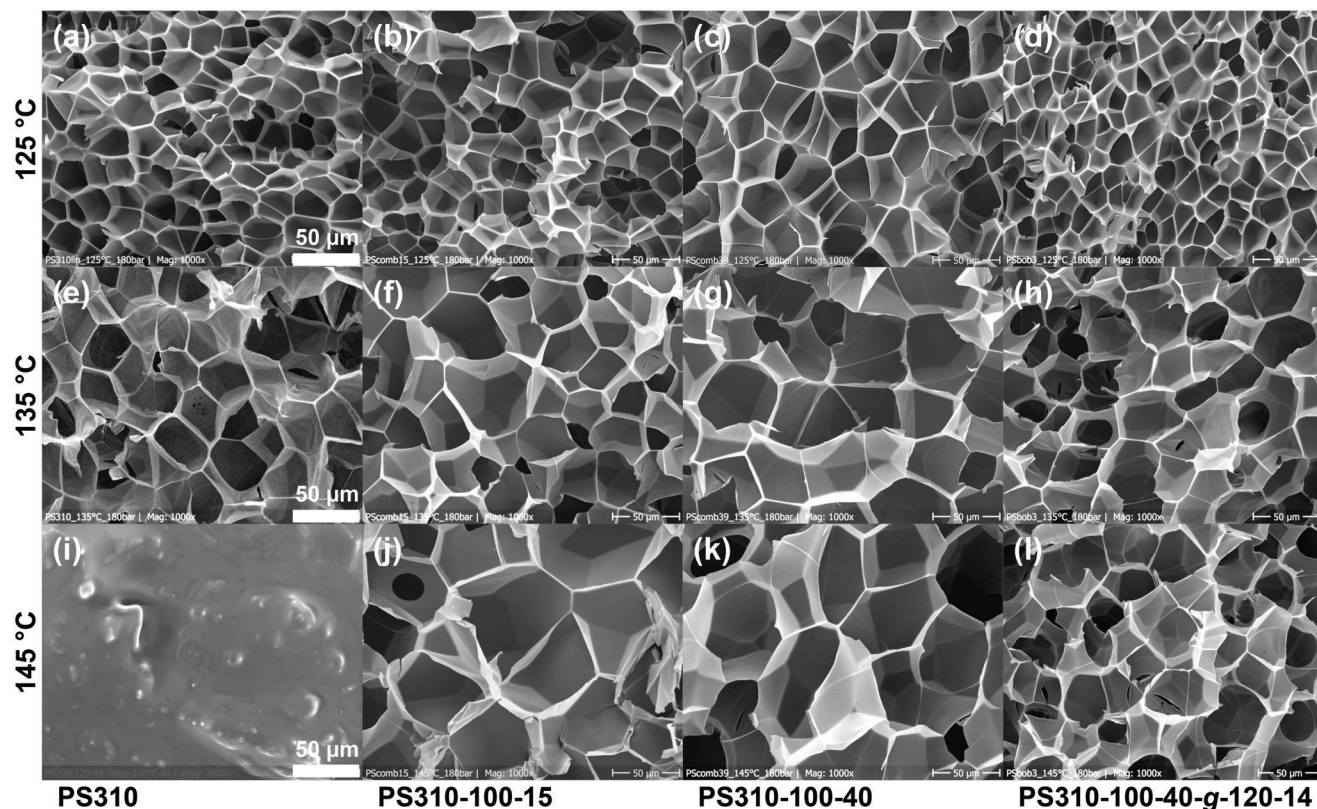


Figure 6. SEM images of the closed cell foam structure of linear PS310, SCB comb PS310-100-15, LCB comb PS310-100-40, and bob PS310-100-40-g-120-40 expanded at 180 bar and a foaming temperature of a–d) 125 °C, e–h) 135 °C, i–l) 145 °C.

process like foaming further influential factors have to be considered. Especially when correlating molecular architecture to in situ processing properties and finding a fingerprint in off-line generated rheological data, it is important that the latter represents the deformational flow field as close as possible.

First of all, parameters like the SHF are strain rate dependent and the applied strain rate or range of strain rates is furthermore individual to the elongational process. During the bubble growth phase, the biaxial extensional flow yields rather high strain rates, $\dot{\epsilon}_H > 0.1 \text{ s}^{-1}$ or even $> 5 \text{ s}^{-1}$.^[47] Since the SCB comb PS310-100-15 displayed a high SHF of 200 at $\dot{\epsilon}_H > 1 \text{ s}^{-1}$ (see Figure 4), and also reached comparably high VER at all foaming conditions, the results suggest a strong correlation between foamability and strain hardening. We assume that the nonlinear field of deformation in the biaxial growth of the bubbles matches also the range of strain rates applied in off-line uniaxial extensional rheology where maximum SHF occurred.^[13] Interestingly, that particular SCB comb PS with barely entangled side chains exhibited the lowest zero-shear viscosity of all investigated samples, $\eta_0 = 5 \times 10^{-4} \text{ Pa s}$, nearly one decade lower than its linear PS310 backbone ($\eta_0 = 4 \times 10^{-5} \text{ Pa s}$), that showed inferior foamability at all temperatures in comparison with the branched samples, i.e., comb or bob PS. Hence, the very low zero-shear viscosity of SCB comb PS310-100-15 does not hinder its expandability and cell stabilizing property in foaming, assumingly because at the later stage of bubble growth, the deformation field is within the nonlinear elongational regime and strain hardening becomes more

important. In this case, a minimum zero-shear viscosity might even expedite the bubble growth.^[48]

Furthermore, LCB comb PS310-100-40 with maximum SHF of 130 and reduced zero-shear viscosity ($\eta_0 = 1 \times 10^{-5} \text{ Pa s}$), compared to the linear PS310, also did show improved expandability. Those findings are in agreement with results from Ab-basi et al.,^[23] who concluded on the basis of the structurally and rheologically similar PS290-120-44 (max. SHF = 200 and max. VER = 40) that a low zero-shear viscosity is certainly not detrimental for foam expansion in case the polymer's structure is inherently strain hardening in the applied region of strain rate at processing conditions.

For the dendrigraft-type bob PS, one would expect that the tremendous strain hardening of SHF of 200–600 at rates $\dot{\epsilon}_H < 0.1 \text{ s}^{-1}$ or even SHF of 1750 at $\dot{\epsilon}_H = 0.005 \text{ s}^{-1}$ translated into an improved stabilization of the cell walls and higher VER as compared to the combs. However, they were not able to outperform comb PS, even though their foamability was better than that of linear PS310. We consider two reasons contributing to this experimental finding. First of all, it can be assumed that the relatively low strain rates of $\dot{\epsilon}_H \leq 0.1 \text{ s}^{-1}$ at which a maximum SHF for bob PS was demonstrated in uniaxial elongational tests did not represent the strain rates occurring in the batch foaming process. At uniaxial experiments conducted at faster stretch times ($\dot{\epsilon}_H > 0.1 \text{ s}^{-1}$) the achieved SHF of 50–200 were still significant, but not remarkably higher than the extensional properties of the SCB or LCB comb PS. In fact, at the highest elongational

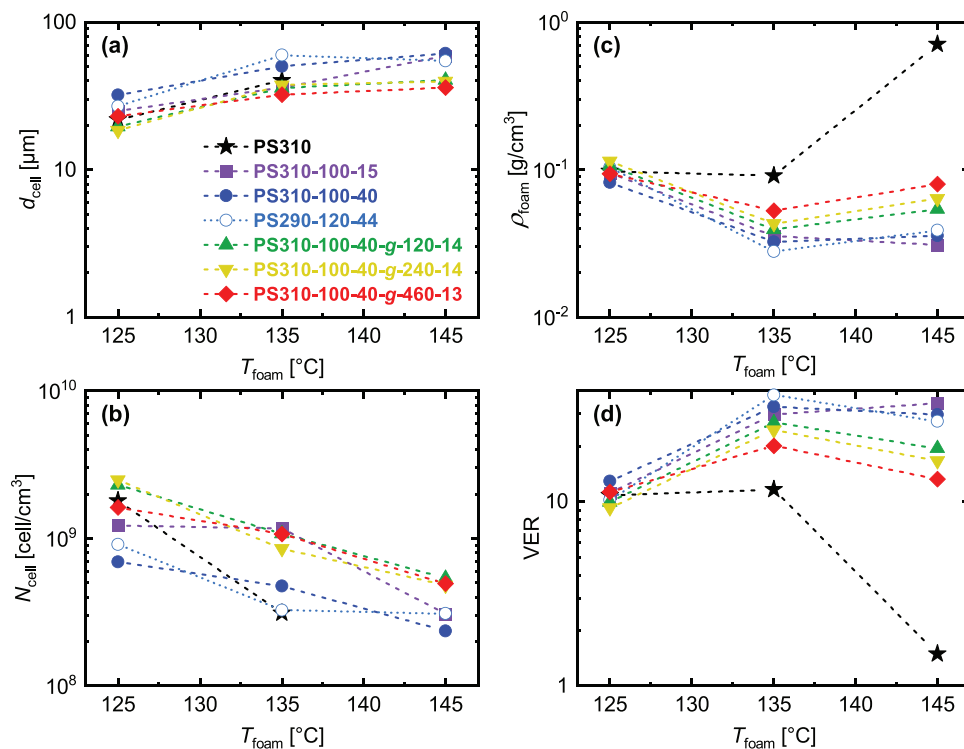


Figure 7. Effect of the temperature on the foaming properties of linear PS310, SCB comb, LCB comb and bob PS310 series, expanded at 180 bar. a) Average cell size, d_{cell} . b) Cell density, N_{cell} . c) Foam density, ρ_{foam} . d) Volume expansion ratio, VER. Dashed lines are guide to the eye. Data of foamed comb PS290-120-44 (open circles) added for comparison from ref. [23]

rates of 3–10 s⁻¹, the SCB comb had the highest strain hardening. It should be noted that bob PS310-100-40-g-120-14 with the lowest graft-density of $N_{\text{scb}} = 120$ not only achieved the highest VER of all bob PS at elevated foaming temperatures (135–145 °C), but furthermore exhibited the highest SHF of all bob samples at nearly all strain rates, and of course also in those regions considered relevant for foaming. Interestingly, both VER as well as SHF decrease in the same order with more outer-branch density from $N_{\text{scb}} = 120$ –460; this behavior might originate from a branch crowding that becomes unfavorable to inter-chain entanglements. This finding would be in agreement with Abbasi et al.^[23] who showed that excessive branching, however, in this case from comb to more densely grafted bottlebrush structures, has a negative impact on extensional processes.

A second contributing factor that bob PS had slightly lower VER than comb PS might be found in their relatively high zero-shear viscosity (Figure S2, Supporting Information). As a retarding force, the zero-shear viscosity affects the bubble growth dynamics in that the gas pressure has to fight against the viscous boundary layer of polymer melt in order to expand the initial bubble nuclei. During the foaming process, the dissolved blowing agent phase separates and the gas concentration within the melt decreases. The loss of the plasticizing effect of the gas leads to a rise in the zero-shear viscosity.^[43,48] Excessive viscosity as an inherent polymer property can suppress bubble growth from the start of depressurization and consequently limit foam expansion.^[49] The time until melt solidification might therefore be shorter for bob PS than comb PS with reduced zero-shear viscosity and probably longer cell growth phase. It needs to be

mentioned that—unlike the undoubted significance of the strain hardening for the melt strength and in foaming—the influence of the zero-shear viscosity here is less evident.

Unfortunately, the influence of branching on the nucleation or bubble growth kinetics could not be covered in the scope of this work, necessitating real-time optical visualization of the foaming process in situ.^[43,50] Therefore, the nucleation densities as well as the cell sizes and their rates of change in the initial foaming stage remain unknown and make it impossible to correlate the cell growth phenomena from the beginning stage with the final foam morphology. For example, higher cell densities and lower cell sizes of bob PS foams—as compared to comb PS (Figure 7a,b)—could have resulted from a higher number of nucleated bubbles, possibly facilitated by effects of branching. Alternatively, as supposed above, a higher zero-shear viscosity could have also caused a decreased bubble growth rate, yielding smaller cells with less strain on the cell walls, i.e., less cell wall rupture, upon earlier melt solidification.

4. Conclusion

A series of three monodisperse dendrigraft polystyrenes with different outer-branch density were synthesized using successive cycles of anionic polymerization, Friedel–Crafts functionalization and grafting-onto methods. Those branch-on-branch (bob) PS were structurally based on a densely grafted comb PS precursor with a well-entangled backbone of $M_{w,bb} = 310 \text{ kg mol}^{-1}$ ($\approx 20 M_e$), and a number of $N_{\text{lc}} = 100$ long chain branches (LCB) of $M_{w,lc} = 40 \text{ kg mol}^{-1}$ ($\approx 3 M_e$). Additional grafting resulted in a

corona of $N_{\text{scb}} = 120, 240,$ and 460 barely entangled short chain branches (SCB) of $M_{\text{w,scb}} \approx 14 \text{ kg mol}^{-1}$ ($\approx 1 M_e$) on the LCB.

Uniaxial extensional properties measured at 180°C were studied in the frameworks of the strain hardening factor (SHF) using an EVF geometry with standard horizontal sample placement as well as tilted by an angle of 20° to allow for higher elongational strains due to the enhanced stretchability of bob PS.

Finally, the samples were foamed in a batch foaming autoclave at 180 bar and a temperature range between 125 and 145°C using CO_2 as the physical blowing agent to study their elongational performance in a processing setup and to correlate elongational rheological with foaming behavior. Special interest was on the expandability, i.e., achieving low dense foams, that directly represents the extensional properties and further originates from the molecular structure.

Analysis of the elongational performance in off-line extensional rheology via the SHF and correlation to the final foam characteristics, especially the volume expansion ratio (VER) resulted in the following conclusions:

- 1) A SHF of 200 at fast Hencky strain rates $\geq 3 \text{ s}^{-1}$ was achieved for a SCB comb PS. Before, this high SHF at Hencky strains below 4 was only reported for LCB combs, however, at lower extensional rates of 0.1 s^{-1} . Both SCB and LCB comb PS achieved maximum VER of $30\text{--}40$, close to a theoretical limit considering the solubility of CO_2 at those foaming conditions.
- 2) Dendrigraft-type bob PS, i.e., SCB grafted onto LCB, reached an exceptionally high SHF of up to 500 at 0.03 s^{-1} , or even 600 at 0.005 s^{-1} were measured using a standard EVF geometry with an instrumentally limited deformation not higher than Hencky strains 4 . To the best of our knowledge, such high strain hardening has never been reported before for polymer melts. This result was achieved for a bob PS having 120 SCB, i.e., in average one SCB per LCB. Within the investigated set of molecular parameters, higher grafting densities showed adverse effects on both SHF as well as VER, assumingly due to excessive branch crowding and a lack of inter-chain entanglements. With a VER of $15\text{--}20$, bob PS showed inferior foam expandability compared to comb PS, even though they outperformed in terms of maximum achievable SHF, however in strain rate regions below 0.1 s^{-1} .
- 3) Using a modified sample placement with a tilted angle of 20° relative to the horizon increased the range of accessible Hencky strains from 4 to 6 . This enabled the viscosity data of highly stretchable bob PS with lowest grafting density of 120 SCB to be recorded for long enough time to reach steady-state in extensional flow, resulting in a maximum SHF of 1750 .
- 4) The quantity of maximum achievable strain hardening alone is not a sufficient criterion for improved foam expansion. Since the SHF is strain rate dependent, off-line extensional rheology can only be correlated to in situ processing properties, if the time scale of deformation in, e.g., foaming is represented by uniaxial elongational tests. In that sense, it can be assumed that the range of strain rates at which SCB and LCB combs show pronounced strain hardening most closely matches the strain rates experienced by the polymer chains close to the melt-gas boundary of the expanding bubbles. Since bubble growth in foaming is a fast extensional process, it is supposed that the cell wall stabilizing effects of strain

hardening do not profit from superior SHF in the range of low strain rates.

This work emphasizes the importance of investigating the structure–property relationship of complex molecular architectures via defined model systems to tune the polymer's molecular parameters according to desired rheological features. The branched architectures exhibit unique rheological properties, especially in elongational melt flow, which play a significant role in polymer processing and, ultimately, material application.

Supporting Information

Supporting Information is available from the Wiley Online Library or from the author.

Acknowledgements

L.F. and M.-C.R. contributed equally to this work. M.A. gratefully acknowledges the Alexander von Humboldt Foundation and the German Research Foundation (DFG, Grant No. WI1911/18-2) for financial support. The authors also gratefully acknowledge the DECHEMA's Max Buchner Research Foundation for research grant. They thank Dr. Carlo Botha for performing SEC measurements with the mixed-bed column, Dr. Miriam Cziep for performing thermorheological stability tests, Dr. Nico Dingenouts for fruitful discussions, and Dr. Michael Pollard for proofreading this article.

Open access funding enabled and organized by Projekt DEAL.

Conflict of Interest

The authors declare no conflict of interest.

Data Availability Statement

The data that support the findings of this study are available from the corresponding author upon reasonable request.

Keywords

comb polymers, dendrigraft branch-on-branch topology, extensional rheology, physical batch foaming, shear rheology, strain hardening factor

Received: June 30, 2022

Revised: September 5, 2022

Published online:

- [1] J. M. Dealy, D. J. Read, R. G. Larson, *Structure and Rheology of Molten Polymers. From Structure to Flow Behavior and Back Again*, Hanser Publications, Cincinnati, OH, USA **2018**.
- [2] a) C. W. Macosko, *Rheology. Principles, Measurements, and Applications*, VCH, New York **1994**; b) H. Münstedt, *Polymers* **2021**, *13*, 1123.
- [3] M. H. Wagner, H. Bastian, P. Hachmann, J. Meissner, S. Kurzbeck, H. Münstedt, F. Langouche, *Rheol. Acta* **2000**, *39*, 97.
- [4] a) S.-T. Lee, C. B. Park, *Foam Extrusion. Principles and Practice*, CRC Press, Boca Raton, FL, USA **2014**; b) S.-T. Lee, C. B. Park, N. S. Ramesh, *Polymeric Foams. Science and Technology*, CRC Press, Boca Raton, FL, USA **2007**; c) N. S. Ramesh, S.-T. Lee, *Polymeric Foams. Mechanisms and Materials*, CRC Press, Boca Raton, FL, USA **2004**.

- [5] G. Liu, H. Sun, S. Rangou, K. Ntetsikas, A. Avgeropoulos, S.-Q. Wang, *J. Rheol.* **2013**, *57*, 89.
- [6] C. R. López-Barrón, M. E. Shivokhin, *Phys. Rev. Lett.* **2019**, *122*, 37801.
- [7] C. R. López-Barrón, M. E. Shivokhin, J. R. Hagadorn, *J. Rheol.* **2019**, *63*, 917.
- [8] F. J. Stadler, A. Nishioka, J. Stange, K. Koyama, H. Münstedt, *Rheol. Acta* **2007**, *46*, 1003.
- [9] D. Ahirwal, S. Filipe, I. Neuhaus, M. Busch, G. Schlatter, M. Wilhelm, *J. Rheol.* **2014**, *58*, 635.
- [10] M. Abbasi, N. Golshan Ebrahimi, M. Wilhelm, *J. Rheol.* **2013**, *57*, 1693.
- [11] M. Abbasi, N. G. Ebrahimi, M. Nadali, M. K. Esfahani, *Rheol. Acta* **2012**, *51*, 163.
- [12] E. Bahreini, S. F. Aghamiri, M. Wilhelm, M. Abbasi, *J. Cell. Plast.* **2018**, *54*, 515.
- [13] J. Stange, H. Münstedt, *J. Rheol.* **2006**, *50*, 907.
- [14] M. S. Kweon, M. Embabi, M. E. Shivokhin, A. Gupta, X. Yan, G. Pehlert, P. C. Lee, *Polymers* **2021**, *14*, 44.
- [15] a) P. Spitael, C. W. Macosko, *Polym. Eng. Sci.* **2004**, *44*, 2090; b) G. J. Nam, J. H. Yoo, J. W. Lee, *J. Appl. Polym. Sci.* **2005**, *96*, 1793; c) J. Stange, H. Münstedt, *J. Cell. Plast.* **2006**, *42*, 445; d) Y. Zhang, P. Tiwary, J. S. Parent, M. Kontopoulou, C. B. Park, *Polymer* **2013**, *54*, 4814; e) P. Pötschke, B. Krause, J. Stange, H. Münstedt, *Macromol. Symp.* **2007**, *254*, 400.
- [16] N. Weingart, D. Raps, M. Lu, L. Endner, V. Altstadt, *Polymers* **2020**, *12*, 725.
- [17] G. Liu, H. Ma, H. Lee, H. Xu, S. Cheng, H. Sun, T. Chang, R. P. Quirk, S.-Q. Wang, *Polymer* **2013**, *54*, 6608.
- [18] M. Abbasi, L. Faust, K. Riazi, M. Wilhelm, *Macromolecules* **2017**, *50*, 5964.
- [19] H. Y. Song, L. Faust, J. Son, M. Kim, S. J. Park, S.-K. Ahn, M. Wilhelm, K. Hyun, *Polymers* **2020**, *12*, 365.
- [20] M. Abbasi, L. Faust, M. Wilhelm, *Adv. Mater.* **2019**, *31*, 1806484.
- [21] a) H. Liang, Z. Cao, Z. Wang, S. S. Sheiko, A. V. Dobrynin, *Macromolecules* **2017**, *50*, 3430; b) J. Paturej, S. S. Sheiko, S. Panyukov, M. Rubinstein, *Sci. Adv.* **2016**, *2*, 1601478; c) H. Liang, B. J. Morgan, G. Xie, M. R. Martinez, E. B. Zhulina, K. Matyjaszewski, S. S. Sheiko, A. V. Dobrynin, *Macromolecules* **2018**, *51*, 10028; d) H. Liang, S. S. Sheiko, A. V. Dobrynin, *Macromolecules* **2018**, *51*, 638.
- [22] M. Abbasi, L. Faust, M. Wilhelm, *Polymer* **2020**, *193*, 122351.
- [23] M. Abbasi, L. Faust, M. Wilhelm, *Polymer* **2020**, *193*, 122354.
- [24] M.-C. Röpert, M. G. Schußmann, M. K. Esfahani, M. Wilhelm, V. Hirschberg, *Macromolecules* **2022**, *55*, 5485.
- [25] a) M. A. Hempenius, W. F. Zoetelief, M. Gauthier, M. Möller, *Macromolecules* **1998**, *31*, 2299; b) E. van Ruymbeke, K. Orfanou, M. Kapnistos, H. Iatrou, M. Pitsikalis, N. Hadjichristidis, D. J. Lohse, D. Vlassopoulos, *Macromolecules* **2007**, *40*, 5941.
- [26] J. H. Lee, K. Orfanou, P. Driva, H. Iatrou, N. Hadjichristidis, D. J. Lohse, *Macromolecules* **2008**, *41*, 9165.
- [27] E. van Ruymbeke, E. B. Muliawan, S. G. Hatzikiriakos, T. Watanabe, A. Hirao, D. Vlassopoulos, *J. Rheol.* **2010**, *54*, 643.
- [28] Q. Huang, S. Costanzo, C. Das, D. Vlassopoulos, *J. Rheol.* **2017**, *61*, 35.
- [29] a) D. Yan, C. Gao, H. Frey, *Hyperbranched Polymers. Synthesis, Properties, and Applications*, Wiley, Hoboken, NJ, USA **2011**; b) D. A. Tomalia, D. M. Hedstrand, M. S. Ferritto, *Macromolecules* **1991**, *24*, 1435.
- [30] M. Seiler, *Fluid Phase Equilib.* **2006**, *241*, 155.
- [31] S. J. Teertstra, M. Gauthier, *Prog. Polym. Sci.* **2004**, *29*, 277.
- [32] a) M. Gauthier, M. Moeller, *Macromolecules* **1991**, *24*, 4548; b) Z. Mughtar, M. Schappacher, A. Deffieux, *Macromolecules* **2001**, *34*, 7595; c) M. Schappacher, J. Bernard, A. Deffieux, *Macromol. Chem. Phys.* **2003**, *204*, 762.
- [33] J. Li, M. Gauthier, *Macromolecules* **2001**, *34*, 8918.
- [34] Z. Yuan, M. Gauthier, *Macromolecules* **2005**, *38*, 4124.
- [35] a) D. A. Tomalia, J. M. J. Fréchet, *J. Polym. Sci., Part A: Polym. Chem.* **2002**, *40*, 2719; b) H. Zhang, Y. Li, C. Zhang, Z. Li, X. Li, Y. Wang, *Macromolecules* **2009**, *42*, 5073.
- [36] a) R. A. Kee, M. Gauthier, *Macromolecules* **2002**, *35*, 6526; b) J. Li, M. Gauthier, S. J. Teertstra, H. Xu, S. S. Sheiko, *Macromolecules* **2004**, *37*, 795; c) R. A. Kee, M. Gauthier, *Macromolecules* **1999**, *32*, 6478; d) M. Gauthier, J. Li, J. Dockendorff, *Macromolecules* **2003**, *36*, 2642; e) H. Zhang, J. Zhu, J. He, F. Qiu, H. Zhang, Y. Yang, H. Lee, T. Chang, *Polym. Chem.* **2013**, *4*, 830.
- [37] D. Parisi, S. Coppola, S. Righi, G. Gagliardi, F. S. Grasso, F. Bacchelli, *Rubber Chem. Technol.* **2022**, *95*, 241.
- [38] a) M. Kempf, D. Ahirwal, M. Cziep, M. Wilhelm, *Macromolecules* **2013**, *46*, 4978; b) K. Riazi, J. Kübel, M. Abbasi, K. Bachtin, S. Indris, H. Ehrenberg, R. Kádár, M. Wilhelm, *Polymer* **2016**, *104*, 240.
- [39] M. Cziep, *private communication*, **2020**.
- [40] P. Hodder, A. Franck, *Annu. Trans. - Nord. Rheol. Soc.* **2005**, *13*, 227.
- [41] a) M. H. Wagner, S. Kheirandish, O. Hassager, *J. Rheol.* **2005**, *49*, 1317; b) Q. Huang, *Macromolecules* **2022**, *55*, 715; c) Q. Huang, M. Mangnus, N. J. Alvarez, R. Koopmans, O. Hassager, *Rheol. Acta* **2016**, *55*, 343; d) Q. Huang, L. Hengeller, N. J. Alvarez, O. Hassager, *Macromolecules* **2015**, *48*, 4158; e) Q. Huang, O. Mednova, H. K. Rasmussen, N. J. Alvarez, A. L. Skov, K. Almdal, O. Hassager, *Macromolecules* **2013**, *46*, 5026.
- [42] a) M. A. Shafi, R. W. Flumerfelt, *Chem. Eng. Sci.* **1997**, *52*, 627; b) M. A. Shafi, J. G. Lee, R. W. Flumerfelt, *Polym. Eng. Sci.* **1996**, *36*, 1950.
- [43] S. N. Leung, C. B. Park, D. Xu, H. Li, R. G. Fenton, *Ind. Eng. Chem. Res.* **2006**, *45*, 7823.
- [44] M. Ataei, V. Shaayegan, C. Wang, F. Costa, S. Han, C. B. Park, M. Bussmann, *J. Rheol.* **2019**, *63*, 895.
- [45] M. H. Wagner, V. H. Rolón-Garrido, J. K. Nielsen, H. K. Rasmussen, O. Hassager, *J. Rheol.* **2008**, *52*, 67.
- [46] a) A. Nishioka, T. Takahashi, Y. Masubuchi, J.-I. Takimoto, K. Koyama, *J. Non-Newtonian Fluid Mech.* **2000**, *89*, 287; b) H. Münstedt, *Int. Polym. Process.* **2018**, *33*, 594.
- [47] a) Z. Xu, Z. Zhang, Y. Guan, D. Wei, A. Zheng, *J. Cell. Plast.* **2013**, *49*, 317; b) K. Taki, K. Tabata, S.-I. Kihara, M. Ohshima, *Polym. Eng. Sci.* **2006**, *46*, 680; c) S.-T. Lee, C. B. Park, *Foam Extrusion*, CRC Press, Boca Raton, FL, USA **2014**.
- [48] Y. Li, Z. Yao, Z.-H. Chen, K. Cao, S.-L. Qiu, F.-J. Zhu, C. Zeng, Z.-M. Huang, *Chem. Eng. Sci.* **2011**, *66*, 3656.
- [49] M. Song, W. Luo, S. Feng, W. Jiang, Y. Ge, T. Liu, *Polymer* **2022**, *238*, 124397.
- [50] a) A. Wong, C. B. Park, *Polym. Test.* **2012**, *31*, 417; b) A. Wong, R. K. M. Chu, S. N. Leung, C. B. Park, J. H. Zong, *Chem. Eng. Sci.* **2011**, *66*, 55; c) V. Shaayegan, G. Wang, C. B. Park, *Eur. Polym. J.* **2016**, *76*, 2; d) Q. Guo, J. Wang, C. B. Park, M. Ohshima, *Ind. Eng. Chem. Res.* **2006**, *45*, 6153; e) R. Deng, T. Jiang, C. Zhang, X. Zeng, B. Liu, J. Yang, S. Li, J. Gu, W. Gong, L. He, *Polymers* **2021**, *13*; f) D. Hu, X. Gao, W. Qiang, Y. Chen, Z. Xu, L. Zhao, *Polym. Test.* **2022**, *105*, 107419; g) S. N. Leung, C. B. Park, H. Li, *Plast., Rubber Compos.* **2006**, *35*, 93.